Available online at www.sciencedirect.com
ScienceDirect
Trans. Nonferrous Met. Soc. China 25(2015) 1752−1762
Transactions of Nonferrous Metals Society of China
www.tnmsc.cn

Influence of thermomechanical processing on microstructure, texture evolution and mechanical properties of Al−Mg−Si−Cu alloy sheets

Xiao-feng WANG, Ming-xing GUO, Ling-yong CAO, Jin-ru LUO, Ji-shan ZHANG, Lin-zhong ZHUANG

State Key Laboratory for Advanced Metals and Materials,
University of Science and Technology Beijing, Beijing 100083, China

Received 18 August 2014; accepted 29 October 2014

Abstract: Influence of thermomechanical processing on the microstructure, texture evolution and mechanical properties of Al−Mg−Si−Cu alloy sheets was studied systematically. The quite weak mechanical properties anisotropy was obtained in the alloy sheet through thermomechanical processing optimizing. The highly elongated microstructure is the main structure for the hot or cold-rolled alloy sheets. H {001}⟨110⟩ and E {111}⟨110⟩ are the main texture components in the surface layer of hot-rolled sheet, while β-fibre is dominant in quarter and center layers. Compared with the hot-rolled sheet, the intensities of β-fibre components are higher after the first cold rolling, but H {001}⟨110⟩ component in the surface layer decreases greatly. Almost no deformation texture can be observed after intermediate annealing. And β-fibre becomes the main texture again after the final cold rolling. With the reduction of the thickness, the through-thickness texture gradients become much weaker. The through-thickness recrystallization texture in the solution treated sample only has cube_{ND} {001}⟨310⟩ component. The relationship among thermomechanical processing, microstructure, texture and mechanical properties was analyzed.

Key words: Al−Mg−Si−Cu alloy; thermomechanical processing; formability; microstructure; texture

1 Introduction

The weight of automobiles continuously decreases during the last 10 years with improving performance, comfort and safety features. Considering the importance of environmental and economical issues, Al−Mg−Si series alloys have been greatly investigated and applied in the automotive industry due to their favorable combination of low specific density, good corrosion resistance, strength and formability. However, their formability still needs to be improved [1−7]. To deal with the formability problem, many researchers have done lots of works consisting of optimizing composition, texture, microstructure and forming parameter [8−10]. It has been demonstrated that the formability of alloy sheet mainly depends on the work hardening coefficient, the strain rate sensitivity and the normal anisotropy, and the last one is greatly influenced by components and density of texture distributed in the alloy.

It is well known that whether the rolling or recrystallization texture is greatly related with the thermomechanical processing applied in the working of Al alloy sheets [5,11−13]. The conventional typical rolling texture of FCC metal is usually dominated by β-fibre, which mainly consists of copper {112}⟨111⟩, S {123}⟨634⟩ and brass {011}⟨211⟩, while the typical recrystallization texture of FCC metal may be comprised of cube {001}⟨100⟩, Goss {110}⟨001⟩, cube_{ND} {001}⟨310⟩, cube_{RD} {013}⟨100⟩, R {124}⟨211⟩, P {011}⟨122⟩ and Q {013}⟨231⟩, which is mainly dependent on the recrystallization mechanism [14−17]. It is a good way to improve the deep drawability by optimizing rolling and recrystallization textures. In addition, it has been found that the deep drawability can be also improved by introducing the γ-fibre consisting of E {111}⟨110⟩ and F {111}⟨112⟩ components in the surface layer of Al alloy sheets. The γ-fibre can be produced through asymmetric rolling [11,12] or changing rolling friction and rolling geometry which is defined as the ratio of projected length of contact between the rolls and material to the mean thickness of

Foundation item: Project (2013AA032403) supported by the National High-Tech Research and Development Program of China, Project (YETP0409) supported by the Beijing Higher Education Young Elite Teacher Project in 2013, China; Project (51301016) supported by the National Natural Science Foundation of China
Corresponding author: Ming-xing GUO; Tel: +86-10-82375844; E-mail: mingxingguo@skl.ustb.edu.cn
DOI: 10.1016/S1003-6326(15)63780-3

the sample (l/d) :

$$l/d=\sqrt{R\Delta h}/[(H+h)/2]=2\sqrt{R(H-h)}/(H+h) \quad (1)$$

where R, Δh, H and h are the roll radius, the thickness reduction per pass, the entry thickness and the exit thickness, respectively. However, it is difficult to obtain γ-fibre texture by conventional thermomechanical processing. Therefore, it is still the best way to improve deep drawability by control microstructure and conventional texture. Considering the genetic effect of texture, in order to obtain an ideal texture component in the solution treated alloy sheets, we must deeply understand the evolution of microstructure and texture during the thermomechanical processing. Unfortunately, these topics still have not been systematically investigated.

The purpose of this work is to understand the influence of thermomechanical processing on the microstructure and texture evolution, and to establish the relationship among thermomechanical processing, microstructure, texture and mechanical properties in the Al−Mg−Si−Cu alloys.

2 Experimental

The chemical composition of the alloy was Al−0.8Mg−0.9Si−0.5Cu−0.2Fe−0.1Mn (mass fraction, %). The ingot with a thickness of 90 mm was melted in a resistance furnace and cast into a preheated steel mould. Subsequently, the ingot was processed as follows: homogenization at 555 °C for 16 h → hot rolling from 90 mm to 7.5 mm at an entrance temperature of 555 °C using a laboratory mill with a roll diameter of 350 mm → cold rolling from 7.5 mm to 4 mm at room temperature using a laboratory mill with a roll diameter of 270 mm → intermediate annealing at 400 °C for 1 h → cold rolling from 4 mm to the final gauge of 1 mm using a laboratory mill with a roll diameter of 270 mm → solution treatment in a salt bath at a temperature of 555 °C for 2 min → water quenching → pre-aging at 80 °C for 12 h + 14 d natural aging (T4P state).

The mechanical properties of the alloy sheet at T4P state, including yield strength (YS), ultimate tensile strength (UTS), elongation, strain-hardening exponent (n) and plasticity strain ratio (r) values, were measured at room temperature in three directions using MTS810 testing machine. Among the above parameters, r value was determined by a tensile strain of 15%.

The Carl. ZEISS Axio Imager A2m optical microscope was used to study the microstructure of the material. The size and distribution of particles before solid solution treatment were investigated through the combination of a SUPRA 55 field emission scanning electron microscope (SEM) equipped with X-ray energy dispersive spectrometer (EDS) and a Tecnai G^2 F30 transmission electron microscope (TEM) equipped with a high angle angular dark field (HAADF) detector and X-ray energy dispersive spectrometer (EDS).

The rolling and annealing textures were determined by measuring {111}, {200}, {220} and {311} incomplete pole figures through D5000 X-ray goniometer using Cu K_α radiation. Orientation distribution functions (ODFs) were calculated from four incomplete pole figures by the series expansion method with l_{max}=22. The position of the layer in the sheet along the vertical direction is indicated by the parameter s which is defined by $s=2\Delta t/t_0$ (t_0 is the sheet thickness, Δt is the distance from the center), and the s values of 0, 0.5, 1, correspond to the center, quarter layer and surface layer, respectively.

The through-thickness recrystallization texture after solid solution treatment was measured by electron backscatter diffraction (EBSD) attached to the SUPRA 55 field emission scanning electron microscope. EBSD sample was prepared by mechanical grinding and electrolytic polishing.

3 Results

3.1 Mechanical property characterization

The detailed mechanical properties of the alloy sheet in the different directions are presented in Table 1. The result shows that the differences in the mechanical properties for the three-direction tension are quite low, indicating the anisotropy has been controlled very well. In addition, normally, the average r and planar anisotropy Δr values are 0.62 and −0.0065, respectively. Obviously, the high average r and low Δr values are beneficial to the deep drawability. Considering the better mechanical properties being related to the microstructure and texture, in order to understand the reasons for the obtained excellent mechanical properties, it is quite necessary to give a systematical characterization on the microstructure and texture.

Table 1 Mechanical properties anisotropy of experimental alloy sheet at T4P state

Direction/(°)	YS/MPa	UTS/MPa	δ/%	n	Average n	r	Average r	Δr
0	145	288	26.4	0.309		0.649		
45	138	276	26.7	0.308	0.308	0.623	0.62	−0.0065
90	141	280	26.0	0.307		0.584		

3.2 Microstructure evolution

The microstructures of the alloy sheet under the different conditions are shown in Fig. 1. After hot rolling from 90 mm to 7.5 mm, the highly elongated microstructure is the main structure in the surface layer and center part, and many coarse particles with average diameter of 10.2 μm distribute along the rolling direction, but the density of particles in the surface layer is much higher (Figs. 1(a) and (b)). After the first cold rolling from 7.5 to 4 mm, the highly elongated microstructure

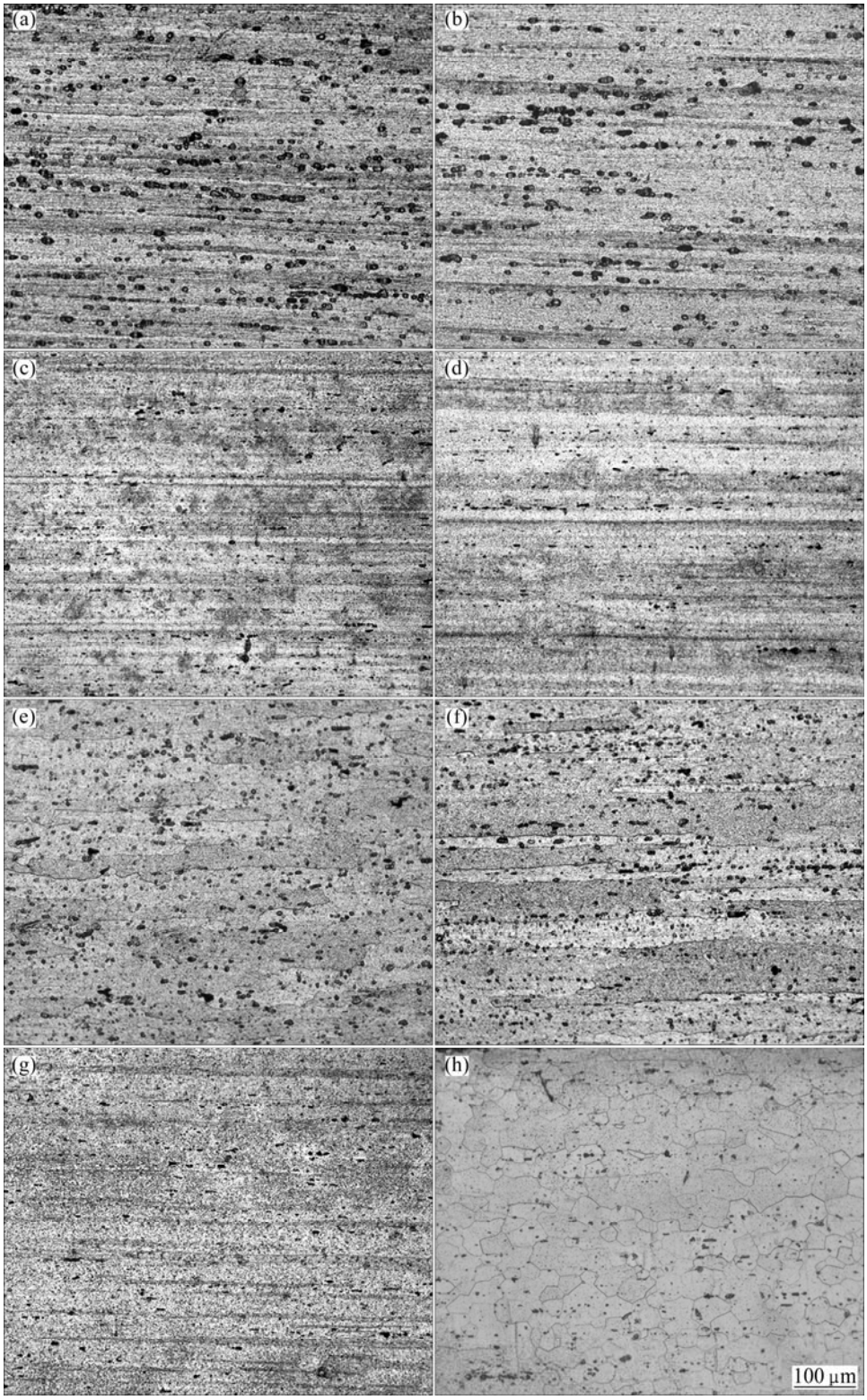

Fig. 1 Optical microstructures of Al−Mg−Si−Cu alloy under different conditions: (a) Surface layer after hot rolling; (b) Center part after hot rolling; (c) Surface layer after first cold rolling; (d) Center part after first cold rolling; (e) Surface layer after intermediate annealing; (f) Center part after intermediate annealing; (g) Final cold rolling; (h) Solid solution

still can be observed, but the coarse particles have been greatly broken even with the deformation of 47% (Figs. 1(c) and (d)). After the intermediate annealing at 400 °C for 1 h, the highly elongated microstructures in the surface layer and center part have been replaced by the coarse recrystallization grains with a high length/width ratio, but the ratio in the surface layer is a little lower (Figs. 1(e) and (f)). Moreover, both the number and average size of the coarse particles increase greatly during the intermediate annealing (Figs. 1(e) and (f)). After the final rolling to the thickness of 1 mm, the highly elongated microstructure was developed again, and the coarse particles formed during the annealing should be broken again and further result in the decrease of their density and size (Fig. 1(g)). After the solid solution treatment, the equiaxed recrystallization grains with an average size of 25 μm can be clearly observed, and the undissolved coarse particles distribute relatively uniformly (Fig. 1(h)).

It is worth noting that the through-thickness microstructure gradient basically can be observed in the hot-rolled, first cold-rolled and intermediate annealed samples, but not in the final cold-rolled and solid solution-treated samples, which is helpful to make a good plan for the further texture characterization.

3.3 Texture evolution

The orientation distribution functions measured from the hot-rolled samples are shown in Fig. 2. It is clearly seen that there is a through-thickness texture gradient in the alloy sheet. The texture components in the surface layer (s=1) mainly include H {001}⟨110⟩ with a high density of 16.2 and E {111}⟨110⟩ with a low density of 2.4, while in the quarter layer, not only H {001}⟨110⟩ but also β-fibre components, such as copper, brass and S, can be observed, their intensities are 2.7, 12.4, 8.0 and 7.9, respectively. The texture in the center part also consists of copper, brass, S and Goss with intensities of 9.7, 10.4, 8.9 and 6.5, respectively. The observed Goss orientation should be attributed to a low deformation in the center part of the hot-rolled sheet [15].

The ODFs in the different layers for the first cold-rolled sample are shown in Fig. 3. Although the cold rolling reduction is about 47% (from 7.5 mm to 4 mm), the through-thickness texture gradient is still significant. β-fibre components become the main texture components in the surface layer, including copper, S and brass with intensities of 7.0, 2.1 and 6.3, respectively. And the retained H {001}⟨110⟩ and {014}⟨145⟩ components with the intensities of 3.8 and 4.2, respectively, can be also observed in the alloy (Fig. 3(a)). The texture in the quarter layer also mainly consists of β-fibre and {016}⟨761⟩ components, but the H {001}⟨110⟩ component has disappeared completely. In the center part, although the β-fibre and Goss components still can be seen, yet, the intensity of Goss component is quite low (Fig. 3(c)).

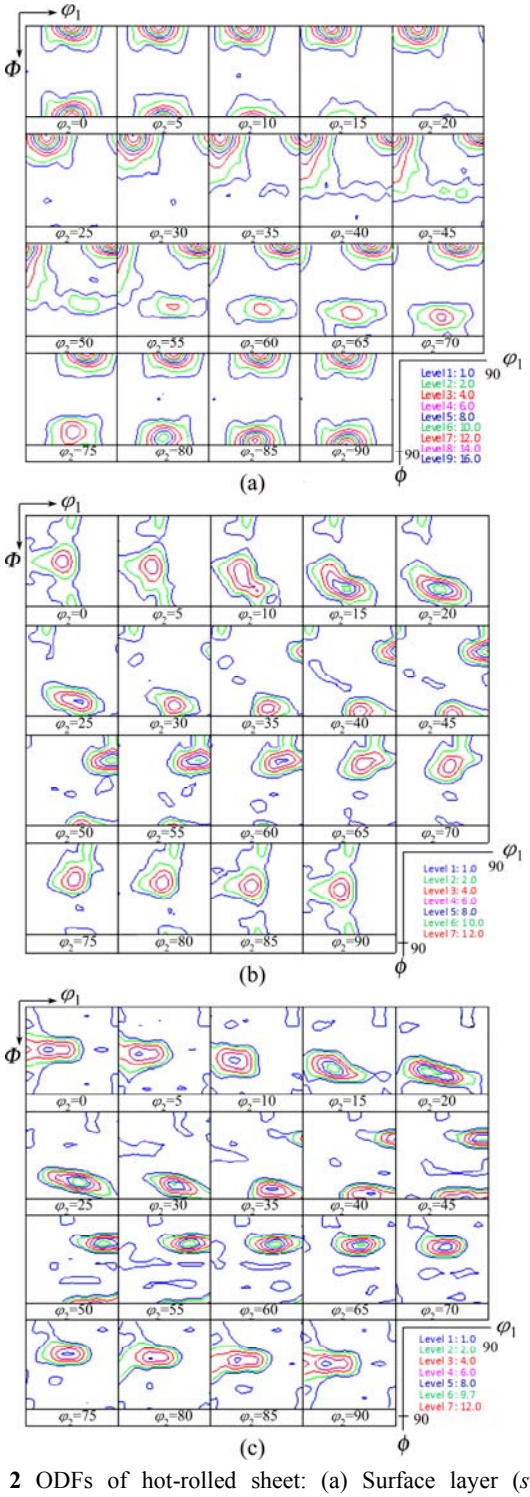

Fig. 2 ODFs of hot-rolled sheet: (a) Surface layer (s=1); (b) Quarter layer (s=0.5); (c) Center part (s=0)

In order to illustrate the through-thickness texture gradients more clearly, the orientation densities along the β-fibre and τ-fibre which run from H {001}⟨110⟩ through copper and to Goss are presented in Fig. 4. From it, it can be clearly seen that although the texture components in

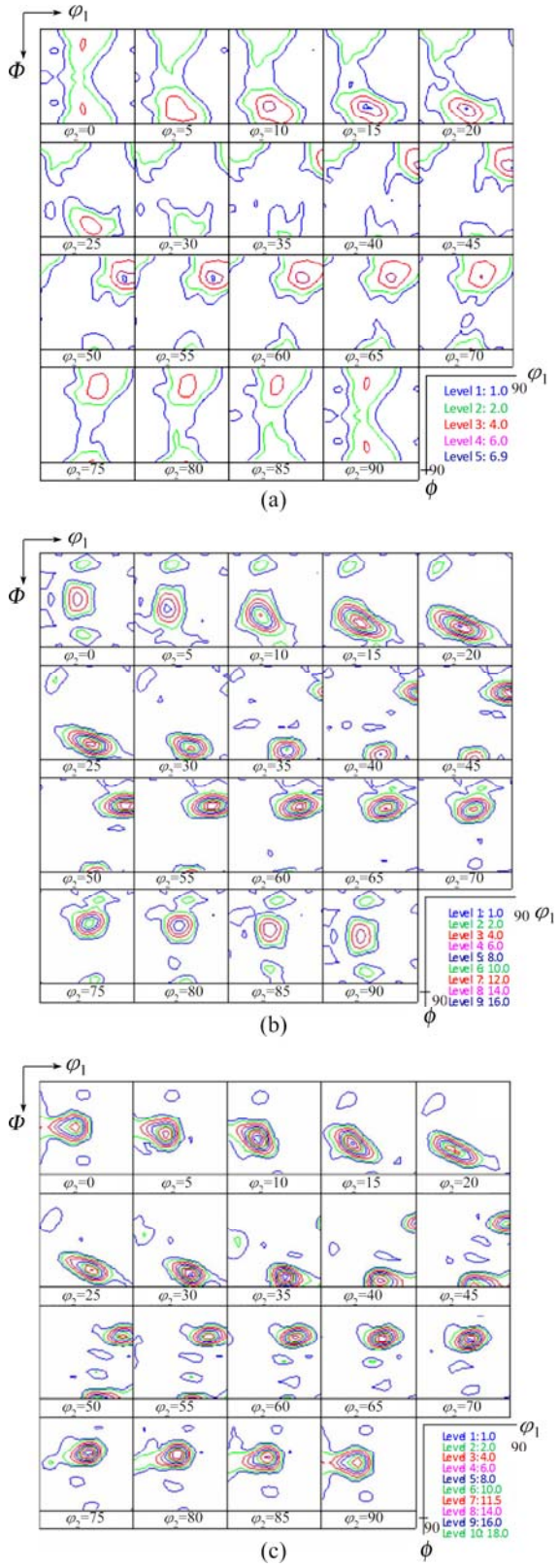

Fig. 3 ODFs of first cold-rolling sheet: (a) Surface layer (s=1); (b) Quarter layer (s=0.5); (c) Center part (s=0)

the center and quarter layers are very similar for the hot-rolled sample, the intensities are quite different, and the copper component increases, whereas the brass component decreases from center part to the quarter

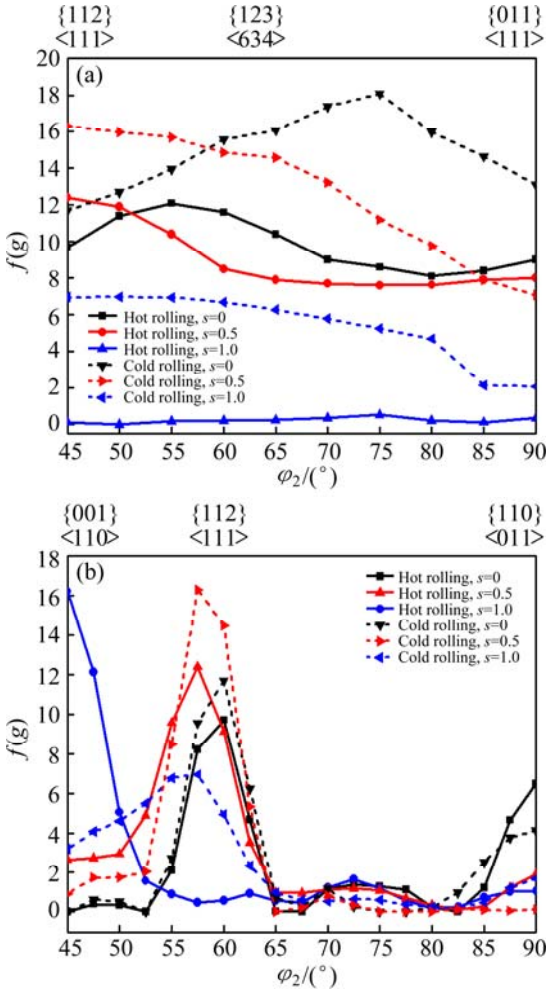

Fig. 4 Orientation densities along different orientations fibers of first cold rolling band in center (s=0), intermediate layer (s=0.5) and surface (s=1): (a) β-fibre; (b) τ-fibre

layer (Fig. 4(a)). In addition, H {001}⟨110⟩ generally increases, whereas the typical deformation texture components decrease from center part to the surface layer (Fig. 4(b)). Compared with the texture components in the hot-rolled sample, the intensities of the observed texture components are basically increased after the first cold rolling (Fig. 4), but H {001}⟨110⟩ component in the surface layer decreases dramatically and mainly transforms to the β-fibre components (Fig. 4(b)). In addition, the Goss component also decreases after cold rolling (Fig. 4(b)).

Figure 5 shows the ODFs of the intermediate annealed alloy sheet. It can be seen that almost all the deformation texture components have transformed into some other components, also including some unusual texture components. The texture in the surface layer consists of cube_{ND} {100}⟨310⟩, cube_{RD} {310}⟨001⟩, Goss, {556}⟨110⟩ and E {111}⟨110⟩ orientations with the intensities of 6.2, 4.1, 2.7, 7.3 and 6.8, respectively. In the quarter layer, the texture components include cube

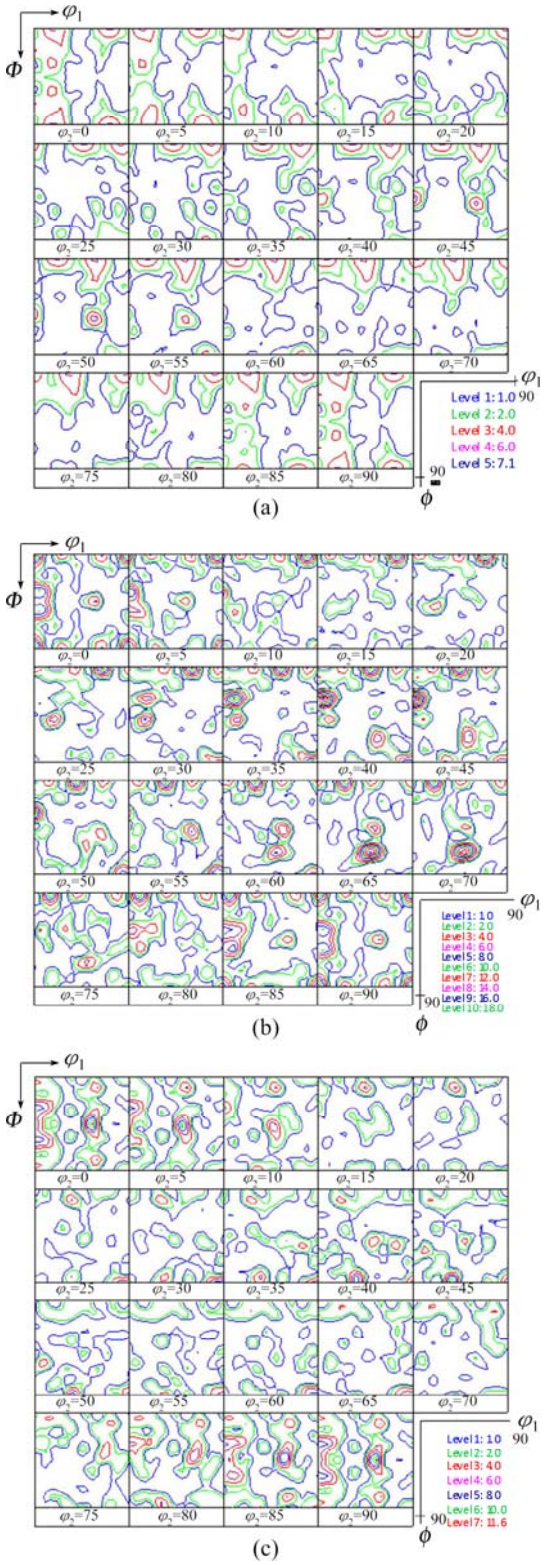

Fig. 5 ODFs of annealed sheet: (a) Surface layer (s=1); (b) Intermediate layer (s=0.5); (c) Center layer (s=0)

{001}⟨100⟩, $cube_{ND}$ {100}⟨310⟩, Goss {110}⟨001⟩, {110}⟨111⟩, {112}⟨110⟩ and {233}⟨145⟩ orientations with intensities of 12.7, 6.3, 6.4, 6.0, 18.3 and 8.1, respectively. While in the center parts, the texture components were changed to {110}⟨111⟩, Q, Goss, {230}⟨235⟩, {110}⟨114⟩ orientations and a rotated cube orientation with a degree of 5° rotated from RD orientation, and their intensities are 12.0, 3.7, 7.4, 3.3, 2.6 and 4.2, respectively. Based on the above results, it can be concluded that the through-thickness texture gradient still exists in the annealed alloy sheet. In addition, although most of the deformation texture components have disappeared after the annealing, the observed texture components are quite different from the typical recrystallization texture components. The main reasons should be resulted from the distribution of dispersion particles or precipitates with the different sizes, and their retard effect on the recrystallization process, especially for the effect on nucleation, growth and orientation rotation of recrystallization grains. Therefore, the observed texture components have orientation differences with the typical texture components.

After the final cold rolling (from 4 mm to 1 mm), the microstructure of the alloy sheet has become quite uniform and basically no microstructure gradient was observed (Fig. 1). Accordingly, we only pay more attention on the texture components in the surface layer significantly affected by friction and other factors. According to the ODF of the final cold-rolled sample (Fig. 6), the retained Goss still can be found, but β-fibre has become the main texture component, and the intensities of its copper, S and brass components are 6.0, 6.3 and 4.5, respectively.

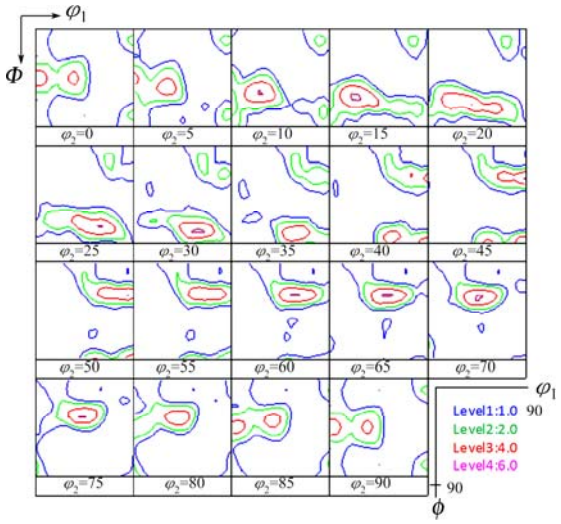

Fig. 6 ODFs of final cold rolling alloy sheet on surface

After the final solid solution treatment, the microstructure and recrystallization grain size distribution were characterized by EBSD (Fig. 7). It can be found that the recrystallization microstructure was controlled very well, the size of most recrystallization grains is about 20 μm and the grain size distribution is relatively uniform, which are beneficial to the

improvement of deep drawability for the experimental alloy. The recrystallization texture is shown in Fig. 8. The ODF reveals that the cube$_{ND}$ {001}⟨310⟩ orientation with a low intensity of 3.8 is the main texture component, and its volume fraction is 11%. The presence of rotated cube component is related with the particle stimulated nucleation during recrystallization.

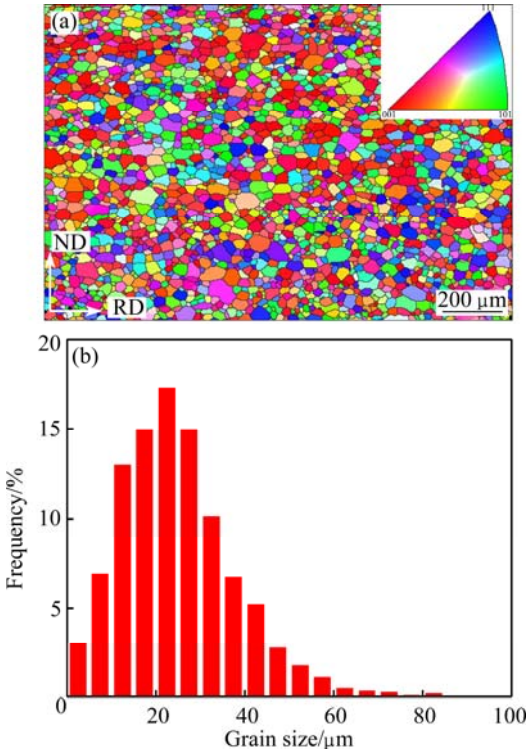

Fig. 7 EBSD analysis of solution treated alloy sheet: (a) IPF map; (b) Grain size distribution

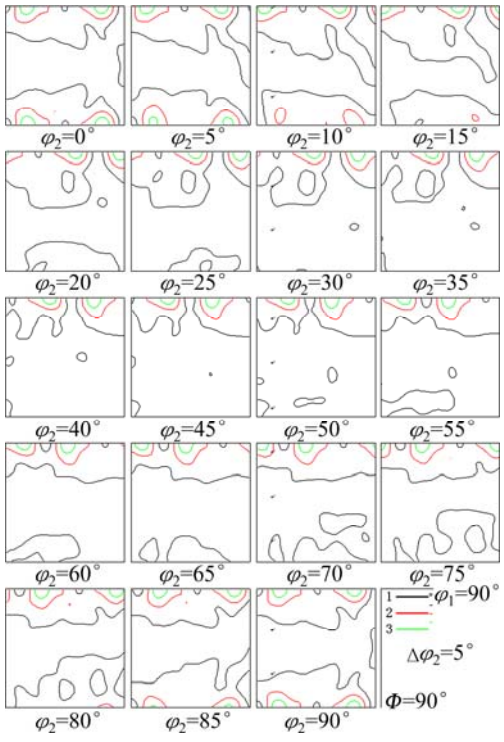

Fig. 8 ODFs of solution treated alloy sheet

4 Discussion

4.1 Effect of rolling geometry

The above experimental results reveal that the through-thickness texture gradients are very obvious in the hot- and cold-rolled bands, and the through-thickness gradients decrease with the decrease of thickness. It is difficult to completely avoid the through-thickness texture gradient and its effect on the following deformation [18−22]. But the texture component and intensity can be controlled and optimized by thermo-mechanical processing. For example, the rolling texture components, H {001}⟨110⟩ and E {111}⟨110⟩, are greatly related with the deformation type and level. Many researchers have pointed out that the rolling texture component is mainly affected by the friction and the rolling geometry. When $1<l/h<5$, the uniform texture can be developed. And when l/h exceeds 5 or is less than 1, the shear texture components can be developed in the surface layer. However, some other people believed that when the rolling reduction is less than 40% per pass or the friction is too small [21−23], the homogeneous textures can be also developed even with very large rolling geometry ($l/h>5$). In addition, MAO [23] suggested that if the friction is high enough or the draught exceeds 40%, the shear texture also can be developed in the surface layer.

The hot rolling geometry and draught are given in Table 2. The rolling geometries for the first five passes are all less than 1 even the corresponding draughts are small, which is beneficial to developing the shear texture. The rolling geometries of the seventh and eighth passes exceed 1 and the draught exceeds 40%, which should be also beneficial to developing shear texture according to Mao's suggestion [23]. The rolling geometry and the draught of the last pass are less than the critical values (l/d=5, draught=40%), which should be impossible to develop shear texture. However, the shear texture can also be developed on the surface after hot rolling (Fig. 2). Similarly, according to the rolling geometries and draughts for all the passes in the first cold rolling (Table 2), they should be beneficial to developing uniform texture but not shear texture. However, some retained shear texture can be observed in the surface layer (Fig. 3). Therefore, the first cold rolling cannot completely remove the shear texture formed in the hot rolling. The shear texture vanishes completely only after the final cold rolling even though the rolling geometries for the last two passes exceed 5, which may be attributed to the good lubricant in the last two passes. Based on the above analysis, we can conclude that even an appropriate rolling geometry is beneficial to develop homogenous texture. It is difficult to remove the formed shear texture

Table 2 Thermomechanical processing parameters of alloy sheet

Treatment	Pass number	Entry thickness/ mm	Exit thickness/ mm	Reduction/ mm	Draught/ %	*l*/*d*
Hot rolling	1	90	84	6	6.7	0.37
	2	84	76	8	9.5	0.47
	3	76	66	10	13.2	0.59
	4	66	56	10	15.2	0.69
	5	56	45	11	19.6	0.87
	6	45	31	14	31.1	1.3
	7	31	18	13	41.9	1.95
	8	18	10	8	44.4	2.67
	9	10	7.5	2.5	25	2.39
First cold rolling	1	7.5	6.8	0.7	9.33	1.36
	2	6.8	6.0	0.8	11.8	1.62
	3	6.0	4.8	1.2	20.0	2.36
	4	4.8	4.0	0.8	16.7	2.36
Final cold rolling	1	4.0	2.8	1.2	30.0	3.74
	2	2.8	2.0	0.8	28.6	4.30
	3	2.0	1.3	0.7	35.0	5.89
	4	1.3	1.0	0.3	23.1	5.53

immediately, which only can be removed gradually with the decrease of the thickness.

4.2 Effect of particles

Large particles, i.e., AlFeMnSi phase, can facilitate the nucleation process of recrystallization (that is particle-stimulated nucleation (PSN)), while small particles, i.e., Mg_2Si or Mn-rich particles, can prevent grain coarsening by retarding the movement of grain boundaries [24,25]. Therefore, the alloy composition and heat treatment should be designed and controlled with an appropriate way. Because particle size and morphology directly affect the texture components and further affect the improvement of the deep drawability, it is important to establish the relationship among the microstructure (particle size, morphology and volume fraction), texture components and deep drawability.

The ability of large particles to act as nucleation sites depends on the particle size (d), the drive pressure for recrystallization (P_D), and the Zener drag due to dispersoids (P_Z). The particle size only follows that particle with a size in excess of d_{crit} will be able to initiate PSN [26,27],

$$d_{crit}=\frac{4\gamma_b}{P_D-P_Z}=\frac{4\gamma_b}{(\alpha\rho Gb^2/2)-(3F_V\gamma_b/d_p)} \quad (2)$$

where γ_b, P_D and P_Z are the specific grain boundary energy, the deformation stored energy and the Zener pinning force exerted by the small particles, respectively. F_V and d_p are the small particle volume fraction and diameter, respectively. It follows from Eq. (2) that the critical nucleation size, d_{crit} increases with the increase of Zener drag P_Z (or decrease of d_p or increase of F_V). Thus, the F_V and d_p of small particles should be also controlled much better, otherwise PSN effect would be suppressed completely when P_Z is large enough. VATNE et al [28] also reported that small particles have a less retarding effect on the nucleation at the cube bands. Accordingly, when P_Z is large enough, cube bands also become the nucleus sites. And the cube orientation would be the main texture component due to the existence of lots of fine particles, its intensity does not decrease even by increasing time and temperature of heat treatment [24,29,30].

Although many coarse particles have been observed in the experimental alloys under different conditions, yet, the kinds, size and volume fraction of observed particles have not been analyzed deeply. Thus, the detailed SEM or TEM microstructure characterization has been conducted. Figure 9 shows that the particles present in the as-deformed state before the solid solution treatment. A large number of large particles with a size of 1.2−25 μm and a spatial density of 10^3 mm^{-2} identified as white AlFeMnSi can be observed. A higher spatial intensity of small particles identified as black Mg_2Si phase is about 1.5×10^4 mm^{-2} (Fig. 9(c)). Small particles are shown more clearly through TEM, as presented in Fig. 10. According to the EDS spectra analysis, the particles mainly consist of lath shaped AlMgSiCu particles and spherical AlFeMnSi particles which were broken during

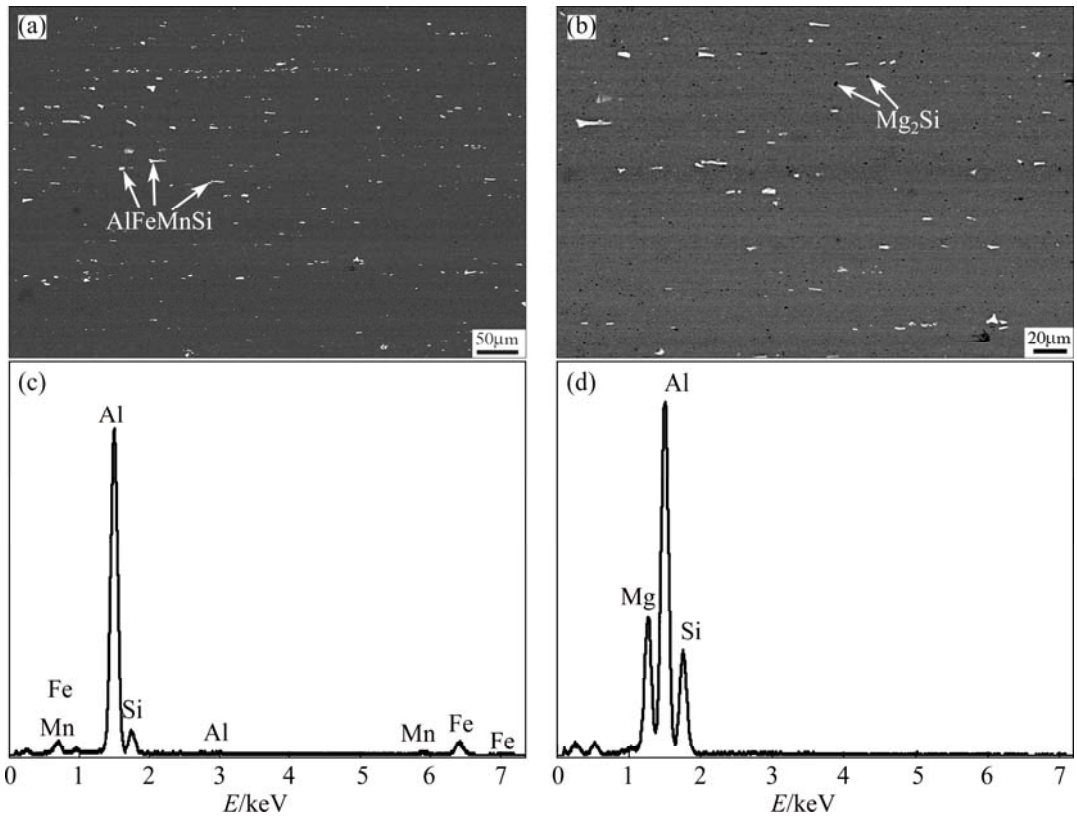

Fig. 9 SEM images (a, b) of sheet before solution treatment and corresponding EDS spectra (c, d) of particles: (a) Large AlFeMnSi particles; (b) Small Mg_2Si particles; (c) White particles, (d) Black particles

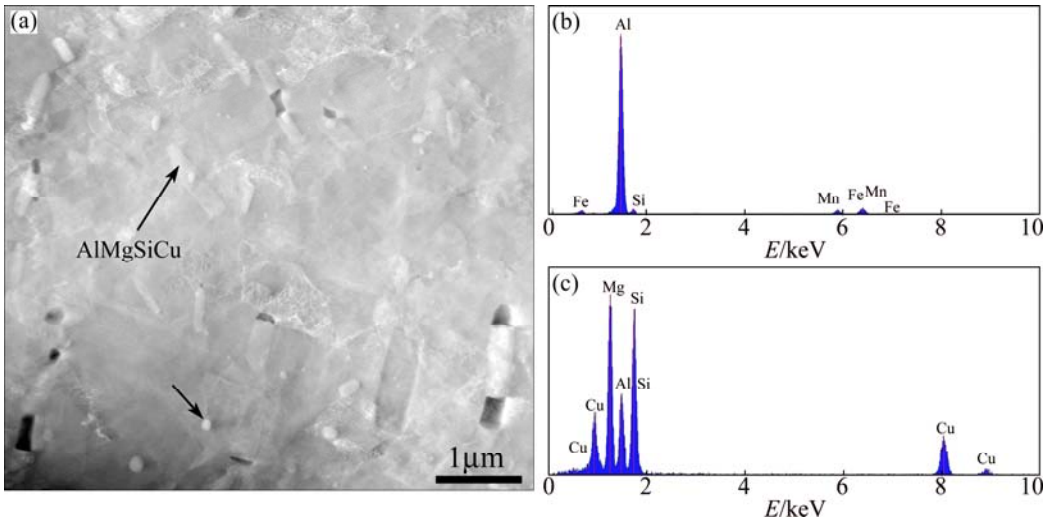

Fig. 10 TEM image (a) of sheet before solution treatment and corresponding EDS spectra (b, c) of particles: (a) Particle distribution; (b) AlFeMnSi particles; (c) AlMgSiCu particles

final cold rolling. Not considering the broken spherical AlFeMnSi particles for such a low intensity, the volume fraction F_V and average size d_p of particles should be around 0.73% and 750 nm, respectively. The ratio of F_V to d_p should be about 0.01 μm^{-1}. Considering lots of fine recrystallization grains resulted from PSN effect have been observed after the solution heat treatment, it can be simply concluded that if the ratio of F_V to d_p is less than 0.01 μm^{-1}, PSN effect would play a key role in the nucleation of recrystallization for the Al−Mg−Si alloy. Accordingly, Fig. 11 gives a schematic illustration of PSN effect on the nucleation and growth of recrystallization grains in the so-called deformation zones of Al−Mg−Si−Cu alloy (black points, black lines

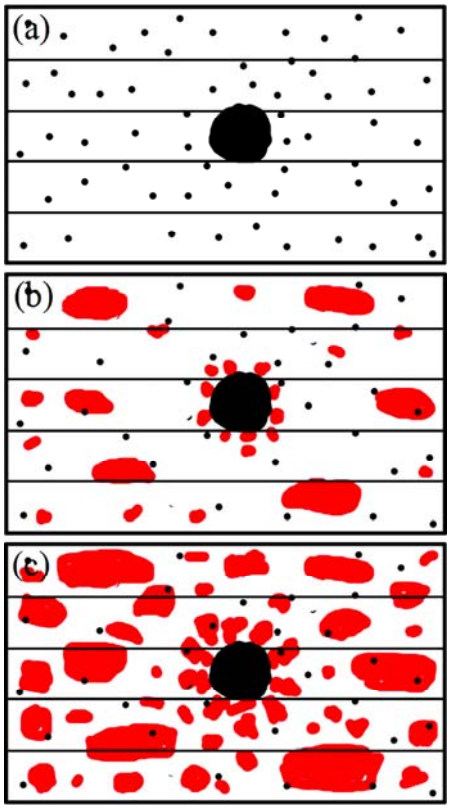

Fig. 11 Schematic illustration of PSN effect on nucleation and growth of recrystallization grains: (a) Before heat treatment; (b) During heat treatment; (c) After heat treatment

and red ones represent particles with different sizes, deformation bands and recrystallization grains).

4.3 Relationship between texture and *r* value

Due to the PSN effect on the recrystallization of alloy, the $cube_{ND}$ {001}⟨310⟩ component with low volume fraction becomes the main texture component after solution treatment, which results in the much higher *r* value for the T4P treated alloy. It has been suggested that the cold rolling type textures balances with certain percentage of cube component can provide an excellent *r* value distribution [31], and *γ*-fibre is also beneficial to improve *r* value of alloy sheet. And certainly, if the recrystallization textures are typically very weak and appear to be almost random, for example, the case observed in the experimental alloy, the formability can be also improved greatly. In addition, LIU et al [31] once pointed out that $cube_{ND}$ {001}⟨310⟩ component possesses low anisotropy that their Δ*r* and average *r* values are less than 1 and more than 0.5, respectively. And the experimental results have confirmed it.

5 Conclusions

1) The quite weak mechanical properties anisotropy, high average *r* and low Δ*r* values have been obtained in the alloy sheet through thermomechanical processing optimizing, which is attributed to the appropriate intensity and component of texture controlled by introducing PSN effect.

2) After hot or cold rolling, the highly elongated microstructure is the main structure in the surface layer and center part, and many coarse particles distribute along the rolling direction. The through-thickness microstructure gradient basically disappears in the final cold-rolled and solution-treated sheets.

3) The hot rolling texture on the surface is mainly comprised of H {001}⟨110⟩ and E {111}⟨110⟩ orientations, while in the other two layers is mainly comprised of *β*-fibre. The intensities of *β*-fibre components are increased after the first cold rolling from 7.5 to 4 mm, but H {001}⟨110⟩ component in the surface layer decreases greatly. Some texture components, i.e., $cube_{ND}$, $cube_{RD}$, Goss form after annealing at 400 °C for 1 h. And *β*-fibre becomes the main texture component again after the final cold rolling from 4 to 1 mm. With the reduction of the thickness, the through-thickness texture gradients become much weaker. The through–thickness recrystallization texture in the solution-treated sheet only has $cube_{ND}$ {001}⟨310⟩ component.

References

[1] BURGER G B, GUPTA A K, JEFFREY P W, LLOYD D J. Microstructural control of aluminum sheet used in automotive applications [J]. Materials Characterization, 1995, 35(1): 23−39.

[2] ENGLER O, HIRSCH J. Texture control by thermomechanical processing of AA6xxx Al−Mg−Si sheet alloys for automotive applications—A review [J]. Materials Science and Engineering A, 2002, 336(1−2): 249−262.

[3] HIRSCH J, AL-SAMMAN T. Superior light metals by texture engineering: optimized aluminum and magnesium alloys for automotive applications [J]. Acta Materialia, 2013, 61(3): 818−843.

[4] GHOSH M, MIROUX A, WERKHOVEN R J, BOLT P J, KESTENS L A I. Warm deep-drawing and post drawing analysis of two Al−Mg−Si alloys [J]. Journal of Materials Processing Technology, 2014, 214(4): 756−766.

[5] SIDOR J, MIROUX A, PETROV R, KESTENS L. Controlling the plastic anisotropy in asymmetrically rolled aluminium sheets [J]. Philosophical Magazine, 2008, 88(30−32): 3779−3792.

[6] HIRSCH J. Recent development in aluminium for automotive applications [J]. Transactions of Nonferrous Metals Society of China, 2014, 24(7): 1995−2002.

[7] LIU Cong-hui, ZHANG Xin-ming, TANG Jian-guo, LIU Xing-xing, CHEN Liang. Effect of copper on precipitation and baking hardening behavior of Al−Mg−Si alloys [J]. Transactions of Nonferrous Metals Society of China, 2014, 24(7): 2289−2294.

[8] HAZRA S, WILLIAMS D, ROY R, AYLMORE R, SMITH A. Effect of material and process variability on the formability of aluminium alloys [J]. Journal of Materials Processing Technology, 2011, 211(9): 1516−1526.

[9] STACHOWICZ F. Formability of aluminium alloy sheets [J]. Journal of Mechanical Working Technology, 1986, 13(2): 229−235.

[10] ZHONG Hao, ROMETSCH P, ESTRIN Y. Effect of alloy

composition and heat treatment on mechanical performance of 6xxx aluminum alloys [J]. Transactions of Nonferrous Metals Society of China, 2014, 24(7): 2174−2178.
[11] SIDOR J, PETROV R H, KESTENS L A I. Deformation, recrystallization and plastic anisotropy of asymmetrically rolled aluminum sheets [J]. Materials Science and Engineering A, 2010, 528(1): 413−424.
[12] SIDOR J, MIROUX A, PETROV R, KESTENS L. Microstructural and crystallographic aspects of conventional and asymmetric rolling processes [J]. Acta Materialia, 2008, 56(11): 2495−2507.
[13] ENGLER O, KIM H C, HUH M Y. Formation of {111} fibre texture in recrystallised aluminium sheet [J]. Materials Science and Technology, 2001, 17(1): 75−86.
[14] HUMPHREYS F J, HATHERLY M. Recrystallization and related annealing phenomena [M]. Pergamon: Elsevier Publishing Company, 2004.
[15] ENGLER O, LÜCKE K. Mechanisms of recrystallization texture formation in aluminium alloys [J]. Scripta Metallurgica et Materialia, 1992, 27(11): 1527−1532.
[16] ENGLER O. Nucleation and growth during recrystallisation of aluminium alloys investigated by local texture analysis [J]. Materials Science and Technology, 1996, 12(10): 859−872.
[17] DOHERTY R D. Recrystallization and texture [J]. Progress in Materials Science, 1997, 42: 39−58.
[18] ASBECK H O, MECKING H. Influence of friction and geometry of deformation on texture inhomogeneities during rolling of Cu single crystals as an example [J]. Materials Science and Engineering A, 1978, 34(2): 111−119.
[19] TRUSZKOWSKI W, KROL J, MAJOR B. Inhomogeneity of rolling texture in fcc metals [J]. Metallurgical Transactions A, 1980, 11(5): 749−758.
[20] TRUSZKOWSKI W, KROL J, MAJOR B. On penetration of shear texture into the rolled aluminum and copper [J]. Metallurgical Transactions A, 1982, 13(4): 665−669.
[21] HUH M Y, CHO Y S, ENGLER O. Effect of lubrication on the evolution of microstructure and texture during rolling and recrystallization of copper [J]. Materials Science and Engineering A, 1998, 247(1−2): 152−164.
[22] VANDERMEER R A. Deformation zone geometry and texture gradients in cold-rolled Niobium [J]. Texture of Crystalline Solids, 1977, 2(3): 183−203.
[23] MAO W. Modeling of rolling texture in aluminum [J]. Materials Science and Engineering A, 1998, 257(1): 171−177.
[24] ENGLER O, HIRSCH J. Recrystallization textures and plastic anisotropy in Al−Mg−Si sheet alloys [J]. Materials Science Forum, 1996, 217−222: 479−486.
[25] ENGLER O. On the influence of dispersoids on the particle stimulated nucleation of recrystallization in an Al−Fe−Si Model Alloy [J]. Materials Science Forum, 1998, 273−275: 483−488.
[26] DAVIES R K, RANDLE V, MARSHALL G J. Continuous recrystallization—Related phenomena in a commercial Al−Fe−Si alloy [J]. Acta Materialia, 1998, 46(17): 6021−6032.
[27] BENNETT T A, PETROV R H, KESTENS L A I. Effect of particles on texture banding in an aluminium alloy [J]. Scripta Materialia, 2010, 62(2): 78−81.
[28] VATNE H E, ENGLER O, NES E. Influence of particles on recrystallisation textures and microstructures of aluminium alloy 3103 [J]. Materials Science and Technology, 1997, 13(2): 93−102.
[29] CHEN Yang, TIAN Ni, ZHAO Gang, LIU Chun-ming, ZUO Liang. Effect of pre-heat treatments on cold rolling and recrystallization textures in Al alloy 6111 [J]. The Chinese Journal of Nonferrous Metals, 2006, 16(8): 1411−1416.(in Chinese)
[30] TROEGER L P, STARKE JR E A. Particle-stimulated nucleation of recrystallization for grain-size control and superplasticity in an Al−Mg−Si−Cu alloy [J]. Materials Science and Engineering A, 2000, 293(1−2): 19−29.
[31] LIU Y S, KANG S B, KO H S. Texture and plastic anisotropy of Al−Mg−0.3Cu−1.0Zn alloys [J]. Scripta Materialia, 1997, 37(4): 411−417.

热加工过程对 Al−Mg−Si−Cu 合金组织、织构演变及力学性能的影响

汪小锋，郭明星，曹零勇，罗晋如，张济山，庄林忠

北京科技大学 新金属材料国家重点实验室，北京 100083

摘　要：系统研究热加工过程对 Al−Mg−Si−Cu 合金组织、织构及力学性能的影响。通过工艺优化获得了力学性能各向异性很弱的合金板材。热轧和冷轧板材的显微组织均呈拉长态组织。热轧板表层的织构组分以 H {001}⟨110⟩ 和 E {111}⟨110⟩为主，而 1/4 层和中间层的织构以 β 取向线为主。与热轧板相比，一次冷轧板的 β 取向线密度增加而表层的 H 取向减弱。经中间退火后，形变织构基本消失，最终冷轧后的织构以 β 取向线为主。随着厚度的减小，织构梯度逐渐变弱。合金板材固溶处理后的再结晶织构组分仅含有 $cube_{ND}$ {001}⟨310⟩织构。此外，分析了热加工过程、显微组织、织构以及力学性能之间的关系。

关键词：Al−Mg−Si−Cu 合金；热加工过程；成形性能；显微组织；织构

(Edited by Xiang-qun LI)